

# Deep Learning Predicts Cardiovascular Disease Risks from Lung Cancer Screening Low Dose Computed Tomography

Hanqing Chao<sup>1</sup>, Hongming Shan<sup>1</sup>, Fatemeh Homayounieh<sup>2</sup>, Ramandeep Singh<sup>2</sup>,  
Ruhani Doda Khera<sup>2</sup>, Hengtao Guo<sup>1</sup>, Timothy Su<sup>3</sup>,  
Ge Wang<sup>1\*</sup>, Mannudeep K. Kalra<sup>2\*</sup>, Pingkun Yan<sup>1\*</sup>

<sup>1</sup>*Department of Biomedical Engineering, Biomedical Imaging Center, Rensselaer Polytechnic Institute, Troy NY 12180, USA*

<sup>2</sup>*Department of Radiology, Massachusetts General Hospital, Harvard Medical School, Boston MA 02114, USA*

<sup>3</sup>*Niskayuna High School, Niskayuna NY 12309, USA*

*\*Asterisks indicate co-corresponding authors*

**The high risk population of cardiovascular disease (CVD) is simultaneously at high risk of lung cancer <sup>1</sup>. Given the dominance of low dose computed tomography (LDCT) for lung cancer screening <sup>2</sup>, the feasibility of extracting information on CVD from the same LDCT scan would add major value to patients at no additional radiation dose. However, with strong noise in LDCT images and without electrocardiogram (ECG) gating, CVD risk analysis from LDCT is highly challenging. Here we present an innovative deep learning model to address this challenge. Our deep model was trained with 30,286 LDCT volumes and achieved the state-of-the-art performance (area under the curve (AUC) of 0.869) on 2,085 National Lung Cancer Screening Trial (NLST) subjects, and effectively identified patients with high CVD mortality risks (AUC of 0.768). Our deep model was further calibrated against the clinical gold standard CVD risk scores from ECG-gated dedicated cardiac CT, including coronary artery calcification (CAC) score <sup>3</sup>, CAD-RADS<sup>TM</sup> score <sup>4</sup> and MESA 10-year CHD risk score <sup>5</sup> from an independent dataset of 106 subjects. In this validation study, our model achieved AUC of 0.942, 0.809 and 0.817 for CAC, CAD-RADS and MESA scores, respectively. Our deep learning model has the potential to convert LDCT for lung cancer screening into dual-screening quantitative tool for CVD risk estimation.**

CVD affects nearly half of American adults and causes more than 30% of fatality <sup>6</sup>. The prediction of CVD risk is fundamental to the clinical practice in manage patient health <sup>7</sup>. Recent studies have shown that the patients diagnosed with cancer have the risk of CVD mortality more than ten-fold greater than that of the general population <sup>8</sup>. However, when the cancer risk population receive screening for cancers, radiologists do not pay attention to their potential CVD risk. For lung cancer screening, LDCT has been proven effective through clinical trials <sup>9,10</sup>. Since the Medicare coverage for LDCT lung cancer screening started in 2015, use of LDCT in eligible high-risk subjects has increased dramatically with 7-10 million scans per year in the United States <sup>2</sup>. Most subjects eligible for lung cancer LDCT screening often have an intermediate to high risk for CVD <sup>1</sup>. It is of great importance for this high-risk population to have an additional CVD screening. The clinical

standard requires a dedicated cardiac CT scan to estimate the CVD risk, which induces a significant cost and high radiation. In contrast, chest LDCT has been shown to contain information especially coronary artery calcification strongly associated with the CVD risk<sup>11</sup>, but there is no consensus of using LDCT images for CVD risk assessment due to the low signal-to-noise ratio and strong image artifacts. This suggests opportunities for advanced systems to tackle the limitations and predict CVD risks from LDCT images.

In the past decade, machine learning, especially deep learning, has demonstrated an exciting potential to detect abnormalities from subtle features of CT images<sup>12</sup>. Several machine learning methods were proposed to estimate CVD factors automatically from CT images. A majority of those methods predict clinically relevant image features including CAC scoring<sup>13–17</sup>, non-calcified atherosclerotic plaque localization<sup>18–22</sup>, and stenosis<sup>23–27</sup> from cardiac CT. None of the existing methods directly estimates the CVD risk from LDCT images which are subject to motion artifacts and low signal-to-noise ratio in contrast to cardiac CT images. Deep learning algorithms were recently applied to quantify CAC scoring from LDCT images as a surrogate of the CVD risk<sup>28–31</sup>. In particular, van Velzen et al.<sup>32</sup> proposed a two-stage method to predict cardiovascular mortality: first extracting image features using a convolutional autoencoder, and then making a prediction using a separate classifier such as a neural network, random forest, or support vector machine. However, such a two-stage method may not be able to extract distinctive features associated with CVD, since the first stage has little knowledge about the final objective. Our previous work showed the feasibility of predicting all-cause mortality risk from patient’s LDCT images from 180 subjects<sup>33</sup>. The developed method, KAMP-Net, first selects a representative 2D key slice from the whole LDCT volume, and then applies an end-to-end CNN to predict all-cause mortality risk (0.76 AUC).

To tackle the limitations of the prior studies, here we build an advanced deep learning approach to predict the CVD mortality risk directly from 3D LDCT images. Most importantly, our proposed approach focuses on the entire cardiac region in a chest LDCT volume for comprehensive analysis of CVD risks. It was then calibrated against the incidents of CVD abnormalities during the follow-up period of a clinical trial, and the CVD risk scores calculated with ECG-gated cardiac CT including the CAC score<sup>3</sup>, CAD-RADS score<sup>4</sup> and MESA 10-year CHD risk score<sup>5</sup>. The proposed deep learning method is built on top of deep convolutional neural networks (CNNs), which are particularly effective in extracting features from images including medical images<sup>34–36</sup>.

Figure 1 shows an overview of the proposed method consisting of three key components in our developed approach. First, a deep CNN based heart detector is trained to isolate the heart region from a chest LDCT volume (Figure 1a). Second, a deep CNN based is designed to compute CVD related features from the entire heart region (Figure 1b). Third, various clinical risk estimators are used for evaluating the developed model on two independent datasets (Figure 1c).

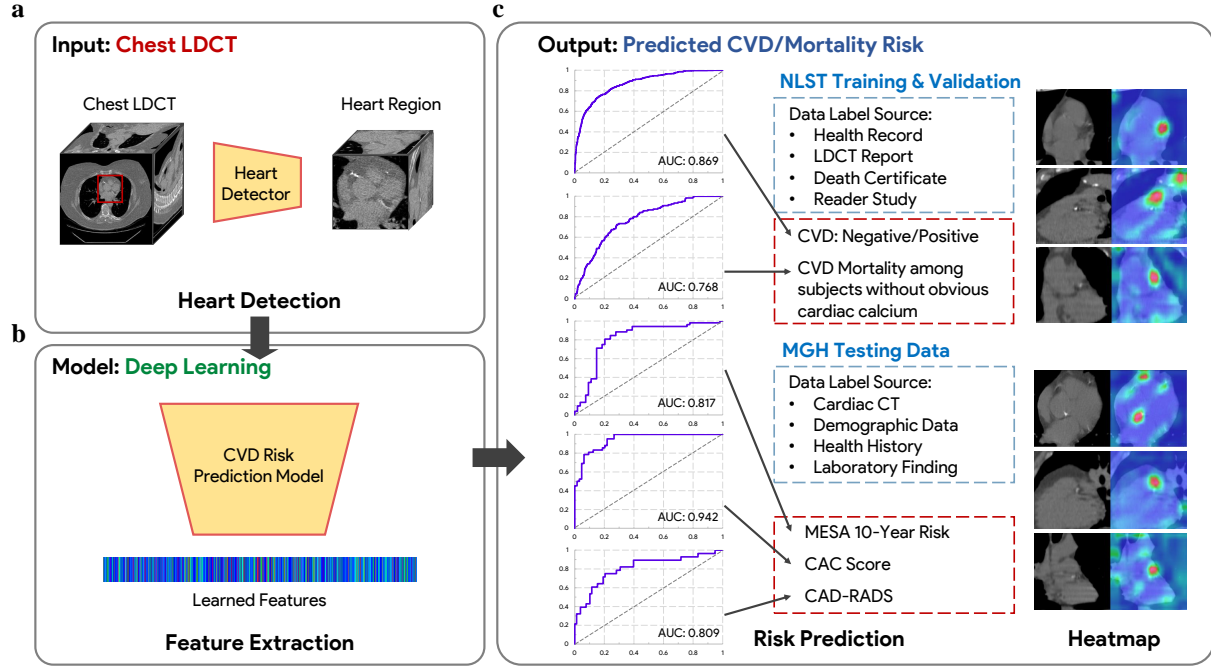


Figure 1: **Overview of the presented deep learning work flow.** The proposed model predicts CVD risks based on 3D chest LDCT images. **a**, The model first extracts the heart region from a chest LDCT volume. **b**, The deep neural network computes radiomic features for CVD risk predictions. **c**, Two independent datasets are used for validation. The model is first evaluated against the clinically reported cardiac abnormalities and then the CVD mortality on the NLST dataset. Also, on our MGH dataset, the learned features are validated against clinical CVD risk scores computed using cardiac CT, including the MESA 10-year risk, CAC score, and CAD-RADS.

## Results

For a systematic characterization, a set of studies were performed on a large number of LDCT images acquired from multiple sources. The datasets and evaluation results are presented as follows.

**Datasets** The first dataset was acquired for the NLST and provided by the National Cancer Institute (NCI). The second dataset was acquired by our team at the MGH. Table 1 summarizes the characteristics of the datasets. In total, we included 6,183 males and 4,318 females aging from 54 to 80, forming a population of 10,501 subjects.

A deep CNN model for CVD mortality risk analysis of LDCT images was designed and trained on the NLST dataset. NLST enrolled in total 26,722 subjects in the LDCT screening arm. Each subject underwent one to three screening LDCT exams, each of which contains multiple CT volumes generated with different reconstruction kernels. We received 47,221 CT exams of 16,264

subjects from NCI, which has reached the maximal number of cases allowed for a public study. Among the available dataset, there are 21,710 exams used in our study from 7,433 normal subjects and 5,189 exams from 2,962 CVD abnormal subjects. The subjects were randomly split into three subsets for training (70%), validation (10%) and testing (20%). The subject assignment was then used to split the LDCT exams into three subsets. Figure 5 shows the inclusion/exclusion criteria and the resultant distribution of LDCT exams in the three subsets (for more details, see Methods, NLST dataset). A subject was considered CVD-positive if any cardiovascular abnormality was reported in the subject's CT screening exams or the subject died of CVD. A CVD-negative subject has no CVD related medical history and no reported cardiovascular abnormality in any of the CT scans during the trial, and did not die of circulatory system diseases.

Furthermore, through an institutional review board (IRB) approved retrospective study, we acquired an independent and fully de-identified dataset from MGH in 2019. This MGH dataset contains 212 imaging examinations of 106 subjects (68 men, 38 women, mean age  $64 \pm 7$  years). Each subject underwent both LDCT for lung cancer screening and ECG-gated cardiac CT for CVD risk assessment. Following the clinical standard protocol, CAC score <sup>3</sup>, coronary stenosis (quantified as CAD-RADS) <sup>4</sup> and MESA 10-year CHD risk <sup>5</sup> were calculated for each subject from cardiac CT. Table 1 lists the characteristics of the dataset (for more details, see Methods, MGH dataset). The dataset was used to evaluate the clinical significance of the model. The model trained on the NLST dataset was directly applied to the LDCT images of this dataset for feature extraction without re-training or fine-tuning.

**Retrospective Findings on NLST** Two experiments were conducted on the NLST dataset, where the proposed deep learning model was compared with other deep learning models and against CAC scores graded by radiologists. Three experienced radiologists from MGH (M.K.K., R.S. and R.D.K.) 2-15 years of clinical experience averaged at 7 years, were assigned to two groups, 1-(M.K.K. and R.S.) and 2-(R.D.K.). Each group independently graded all the 2,085 CT volumes to obtain the CAC grades. Four CAC categories were used, including no calcification (level 0 - normal), calcifications over less than one-third of the length of coronary arteries (level 1 - minimal), calcifications over 1/3 to 2/3 of the coronary arterial lengths (level 2 - moderate) and calcifications greater than 2/3 of the arterial length (level 3 - heavy). The average reader results are calculated by averaging the results of the two groups. The first experiment evaluated the proposed model for its capability in identifying patients with CVD diseases from the lung cancer screening population on the entire test set of 2,085 subjects. The receiver operating characteristic curves (ROCs) of multiple methods in this experiment are shown in Figure 2a. The model achieved an area under the curve (AUC) value of 0.869 (95% confidence interval, 0.854-0.886)(see Methods, Statistical analysis). With a positive predictive value (PPV) of 50.00%, the model achieved a sensitivity of 88.03%, which suggests that the deep learning model can correctly identify 88.03% of the CVD-positive subjects using only a chest LDCT scan, when allowing half of the positive predictions false. For the reader performance, all patients with CAC level 1 and above (CAC Grade 1+) are considered as abnormal. It can be seen in Figure 2a that CAC Grade 1+ yielded a sensitivity of 96.0% and a PPV of 36.8%. While our model has a similar sensitivity of 96.6%, it achieved a higher PPV of 37.2% ( $p=0.3847$ ). In addition,

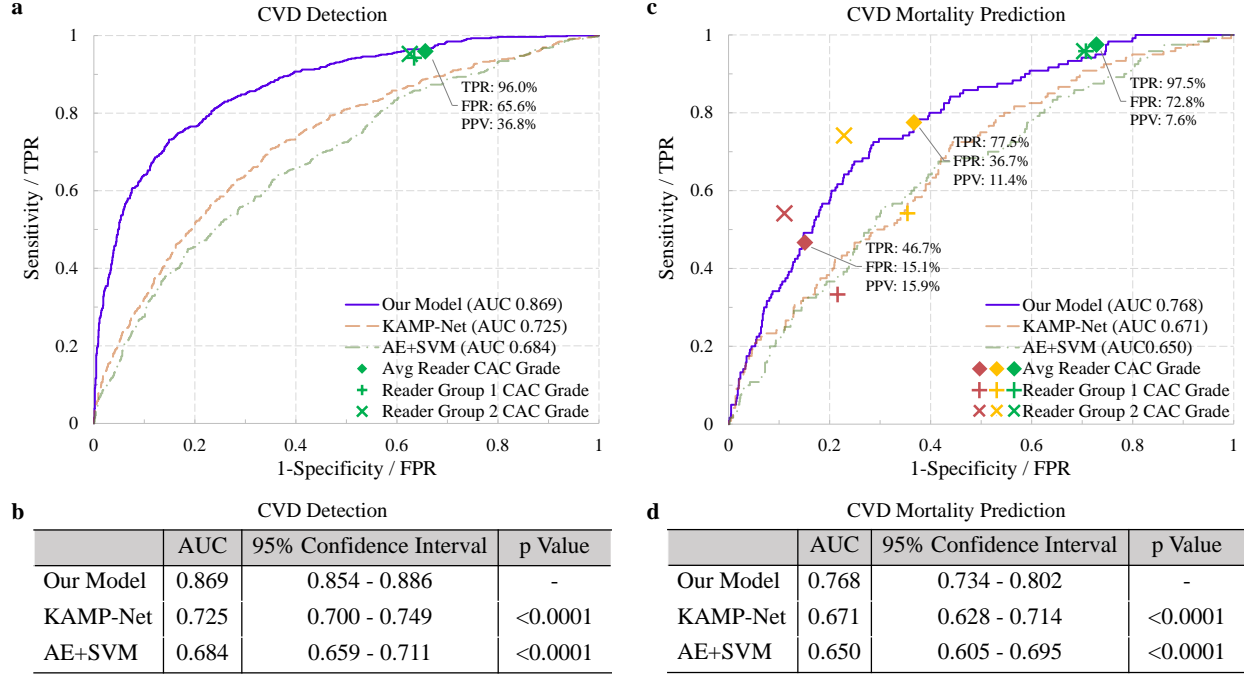


**Figure 2: Experimental results on the NLST dataset. a & b,** Comparison of our model with other reported methods on CVD detection using the full NLST test set including 2,085 subjects. **c & d,** Reader study and comparison of our model with other reported methods on CVD caused mortality prediction. For reader study in **a & c**, red symbols represents CAC Scores 1+, yellow symbols represents CAC Scores 2+, green symbols represents CAC Scores 3.

we compared our model with the two recently reported works, KAMP-Net<sup>33</sup> and Auto-encoder (AE+SVM)<sup>32</sup>. The table in Figure 2b shows that our model significantly outperformed the other two methods ( $p < 0.0001$ ). It indicates that our deep CNN model can differentiate subjects with high CVD risk from others with low risk using LDCT images alone.

In our second experiment, we evaluated the performance of the deep learning model against human experts in CVD related mortality prediction. Among these 2,085 test subjects, 120 subjects died of CVD during the trial. The objective was to predict the mortality of those 120 subjects based on their LDCT images. The expert estimated CAC grades were used to predict the CVD caused mortality and the results are shown in Figure 2c. The performance of CAC Grade 1+, 2+, and 3 indicates using categories 1 and above, categories 2 and above, and 3 only, respectively, to consider as mortality. The trained deep learning model was directly applied to this testing set to predict the CVD-caused mortality without fine-tuning. Our deep learning model achieved an AUC value of 0.768 (95% confidence interval, 0.734-0.802), which significantly outperformed the competing methods ( $p < 0.001$ ) as shown in Figure 2c,d. Additionally, it can be seen from Figure 2c that our model achieved a similar performance with the top human experts' average performance. Although the performance of reader group 2 is higher than our model, there is a significant difference between

the two groups' annotation ( $p < 0.0001$ ). The average per-case difference is 0.34. As in clinical practice, each LDCT examination is usually reported by one radiologist, our model could provide a more reliable result. The model can help make interpretation more efficient while reducing inter-and intra-observer variations in quantifying CAC. The model can also automate and quantitate CVD risk categorization so that radiologists can focus on other tasks such as lung nodule detection, measurement, stability assessment, classification (based on nodule attenuation) and other incidental findings in the chest and the upper abdomen.

### **Comparison of Deep Learning on LDCT Against Gold Standard CVD Risk Factors on CCT**

To investigate the generalizability of our AI model and further evaluate the reliability of the deep learning model against gold standard CVD risk factors, three studies were conducted on the MGH dataset. This IRB approved study included 106 patients from MGH who underwent LDCT for lung cancer screening and had a separate ECG-gated coronary calcium scoring CT as well as a coronary CT angiogram (CCT) for CVD diagnosis. More details are presented in Methods. Table 1 lists the characteristics of the dataset. Two thoracic radiologists qualitatively graded the extent of CAC on LDCT images using the same method as described in the NLST dataset (4 levels, i.e., level 0 - normal, level 1 - minimal, level 2 - moderate, and level 3 - heavy). The coronary calcium scoring CT images were processed using a commercial software as per the standard of care at MGH (Syngo Via, Siemens Healthineers) according to the standard clinical protocol<sup>3</sup>. Using patient characteristics (age, gender and race) and CAC scores, we estimated the Multi-ethnic Scores for Atherosclerosis (MESA) based 10-year risk (MESA score)<sup>5</sup>. In addition, two cardiac radiologists reviewed coronary CT angiogram classified the luminal patency or stenosis of coronary arteries on the basis of the Coronary Artery Disease Reporting and Data Systems (CAD-RADS<sup>TM</sup>) score<sup>4</sup>. Both CAC and CAD-RADS scores are established clinical methods for assessing CVD.

In all these three experiments, our deep learning model was trained on the NLST data as described earlier, and then directly applied to the MGH data for feature extraction without further training nor fine-tuning. The extracted features from LDCT were used to estimate the clinical risk scores for comparison through logistic regression. Five-fold cross validation was used in all the experiments. Our model was also compared with the radiologists' CAC grades and the two previous studies on CVD risk prediction<sup>32,33</sup>. The CAC grades were directly used to predict different CVD factors. Like in the NLST experiments, the performance of CAC Score 1+, 2+ and 3 was calculated. Our experimental results are presented as follows.

The features extracted by the deep learning model from LDCT were first used to estimate the CAC scores through logistic regression. With a threshold of Agatston score 400, the MGH subjects were divided into two groups, with (42 subjects) or without (64 subjects) severe CAC. Our model achieved an AUC value of 0.942 (95% confidence interval, 0.919-0.965) and significantly exceed the results using the other two methods ( $p < 0.0001$ , see Figure 3d) and is competitive with radiologists' performance. The AUC for our DL model was slightly lower compared with the radiologists' CAC grading. This could have resulted from lack of training of our DL model with CAC score estimation or from the limitation of dataset and high dimension of the DL features

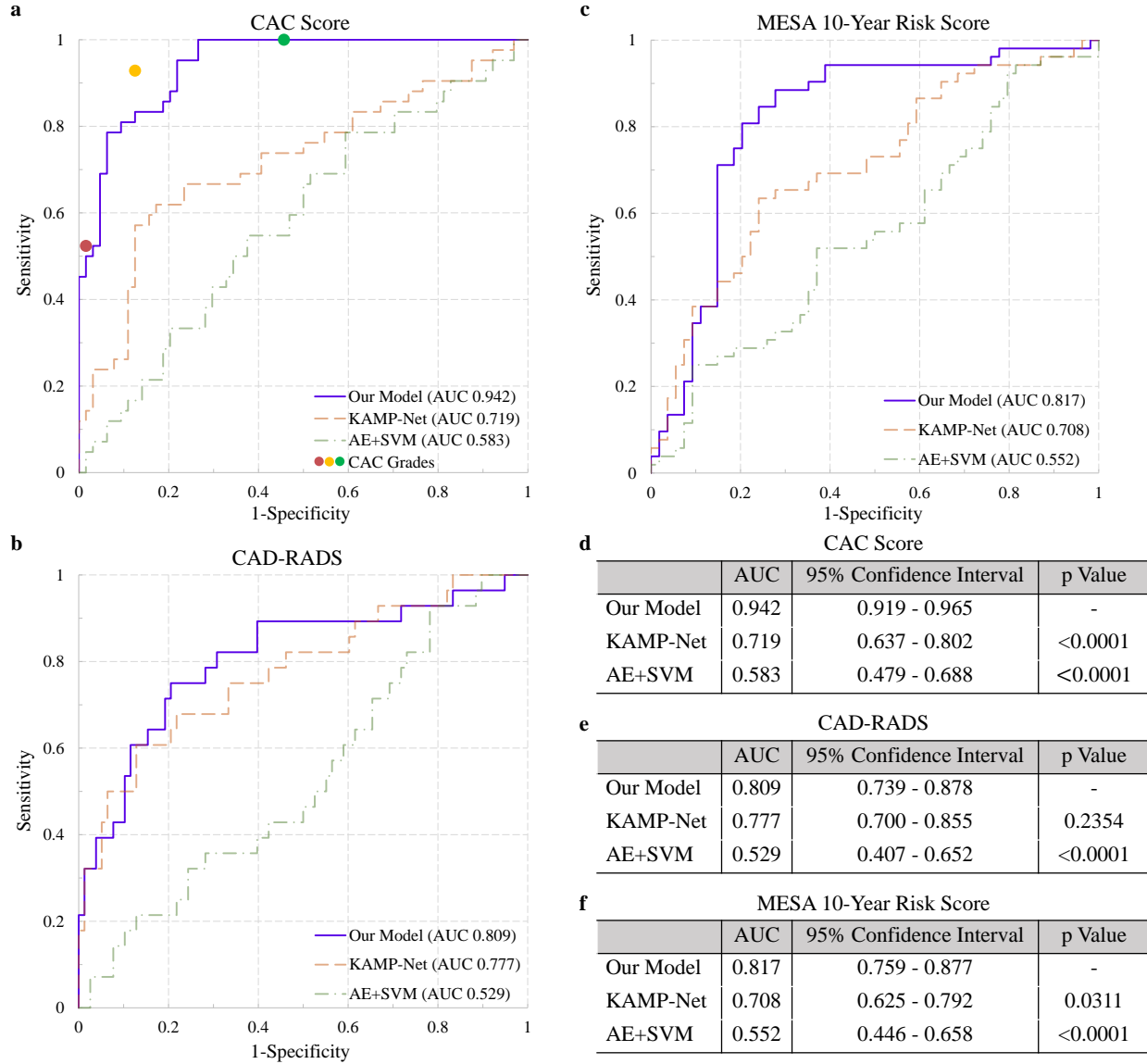


**Figure 3: Results of deep learning on LDCT against human experts on CCT using the MGH dataset.** Comparison of our deep learning model with three clinical standard criteria the CAC score<sup>3</sup>, CAD-RADS<sup>4</sup> and MESA 10-year risk score<sup>5</sup> calculated with the standard protocol by radiologists. The comparison is performed on n=106 cases. **a & d**, Comparison of the model performances of the CAC score. **b & e**, Comparison of the model performance on fitting CAD-RADS. **c & f**, Comparison of the model performance in terms of the MESA score. For radiologists' CAC grades in **a**, red dots represents CAC Scores 1+, yellow dots represents CAC Scores 2+, green dots represents CAC Scores 3.

leading to an overfitting of the linear logistic regression. The data suggest that deep learning using LDCT can well approximate the human expert performance using CCT in differentiating patients

with severe and non-severe CAC. The ROC curves are shown in Figure 3a.

The second experiment evaluates the capability of the deep learning model in classifying subjects to high and low risk groups using LDCT by comparing against the coronary stenosis (CAD-RADS) scores obtained by human experts on CCT. The subjects with CAD-RADS score equal or larger than 4 are labeled as severe stenosis, *i.e.*, positive samples (28 subjects). Other subjects with smaller scores were labeled as negative (78 subjects). Our model reached an AUC value of 0.809 (95% confidence interval, 0.919-0.965, see Figure 3b,e), which is very encouraging with the use of LDCT. Our model significantly outperformed AE+SVM<sup>32</sup> ( $p < 0.0001$ ). Different from calcification, coronary stenosis is much harder to detect through a chest LDCT screening, while it is a direct biomarkers of CVD risk. The superiority on this task means that in CVD risk estimation, our model can quantify the subclinical imaging markers on LDCT, which makes it a promising tool for CVD assessment in lung cancer screening.

In the third experiment, patients are divided into high and low risk groups according to their MESA 10-year risk scores which is a clinical standard CVD risk criterion on integrating multiple factors including gender, age, race, smoking habit, family history, diabetes, lipid lowering and hypertension medication, CAC score extracted from CCT, and laboratory findings including cholesterol and blood pressure. With a threshold of 14.2, 52 subjects were labeled as high risk while 54 subjects were labeled as low risk. Our model achieved an AUC value of 0.817 (95% confidence interval, 0.759-0.877), which significantly outperformed all the other methods (see Figure 3c,f).

In summary, our deep learning model enhances the value of CVD risk estimation from LDCT for lung cancer screening. Given the increasing utilization of LDCT-based lung cancer screening, and shared risk factors and high prevalence of CVD in these at-risk patients, our model obviates the need for an additional screening method in these patients by obtaining a quantitative and reliable CVD risk prediction. Comparable or superior performance of our model (AUC of 0.783) from LDCT imply that additional dedicated ECG-gated coronary calcium scoring, and other laboratory tests can be avoided. Our deep learning-model can not only reduce the cost and radiation dose in workup of at-risk patients for CVD, but also improve patient compliance with screening by maximizing the return of crucial quantitative information from a single, low-dose test. Given the technical challenges associated with quantification of CAC from LDCT for lung cancer screening versus ECG-gated cardiac CT, our study marks an important development in obtaining crucial CVD-related risk information from LDCT for lung cancer screening. The trained models could aid clinicians in estimating the risk of CVD for patients who undergo LDCT exams. The further comparative study on the deep learning model of LDCT images with human experts on CCT for risk group classification shows that the deep learning model can just analyze LDCTs to well approximate the clinical reading with dedicated cardiac CTs.



## References

1. Hecht, H. S., Henschke, C., Yankelevitz, D., Fuster, V. & Narula, J. Combined detection of coronary artery disease and lung cancer. *European Heart Journal* **35**, 2792–2796 (2014).
2. Chin, J. *et al.* Screening for Lung Cancer with Low-Dose CT Translating Science into Medicare Coverage Policy. *New England Journal of Medicine* **372**, 2083–2085 (2015).
3. Agatston, A. S. *et al.* Quantification of coronary artery calcium using ultrafast computed tomography. *Journal of the American College of Cardiology* **15**, 827–832 (1990).
4. Cury, R. C. *et al.* CAD-RADS<sup>TM</sup> coronary artery disease–reporting and data system. an expert consensus document of the Society of Cardiovascular Computed Tomography (SCCT), the American College of Radiology (ACR) and the North American Society for Cardiovascular Imaging (NASCI). Endorsed by the American College of Cardiology. *Journal of cardiovascular computed tomography* **10**, 269–281 (2016).
5. McClelland, R. L. *et al.* 10-year coronary heart disease risk prediction using coronary artery calcium and traditional risk factors. *Journal of the American College of Cardiology* **66**, 1643–1653 (2015).
6. Benjamin Emelia J. *et al.* Heart Disease and Stroke Statistics 2019 Update: A Report From the American Heart Association. *Circulation* **139**, e56–e528 (2019).
7. Raghunath, S. *et al.* Prediction of mortality from 12-lead electrocardiogram voltage data using a deep neural network. *Nature Medicine* 1–6 (2020). URL <https://www.nature.com/articles/s41591-020-0870-z>. Publisher: Nature Publishing Group.
8. Sturgeon, K. M. *et al.* A population-based study of cardiovascular disease mortality risk in US cancer patients. *European Heart Journal* **40**, 3889–3897 (2019).
9. Bach, P. B. *et al.* Benefits and Harms of CT Screening for Lung Cancer: A Systematic Review. *JAMA* **307**, 2418–2429 (2012).
10. National Lung Screening Trial Research Team *et al.* Reduced lung-cancer mortality with low-dose computed tomographic screening. *The New England Journal of Medicine* **365**, 395–409 (2011).
11. Chiles, C. *et al.* Association of Coronary Artery Calcification and Mortality in the National Lung Screening Trial: A Comparison of Three Scoring Methods. *Radiology* **276**, 82–90 (2015).
12. Ardila, D. *et al.* End-to-end lung cancer screening with three-dimensional deep learning on low-dose chest computed tomography. *Nature Medicine* **25**, 954–961 (2019).
13. Liu, Q. *et al.* Lesion-specific coronary artery calcium quantification for predicting cardiac event with multiple instance support vector machines. In *International Conference on Medical Image Computing and Computer-Assisted Intervention*, 484–492 (Springer, 2010).

14. Işgum, I., Prokop, M., Niemeijer, M., Viergever, M. A. & Van Ginneken, B. Automatic coronary calcium scoring in low-dose chest computed tomography. *IEEE transactions on medical imaging* **31**, 2322–2334 (2012).
15. Wolterink, J. M., Leiner, T., Takx, R. A., Viergever, M. A. & Işgum, I. Automatic coronary calcium scoring in non-contrast-enhanced ecg-triggered cardiac ct with ambiguity detection. *IEEE transactions on medical imaging* **34**, 1867–1878 (2015).
16. Yang, G. *et al.* Automatic coronary calcium scoring using noncontrast and contrast ct images. *Medical physics* **43**, 2174–2186 (2016).
17. Wolterink, J. M. *et al.* Automatic coronary artery calcium scoring in cardiac ct angiography using paired convolutional neural networks. *Medical image analysis* **34**, 123–136 (2016).
18. Zuluaga, M. A., Hush, D., Leyton, E. J. D., Hoyos, M. H. & Orkisz, M. Learning from only positive and unlabeled data to detect lesions in vascular ct images. In *International Conference on Medical Image Computing and Computer-Assisted Intervention*, 9–16 (Springer, 2011).
19. Yamak, D., Panse, P., Pavlicek, W., Boltz, T. & Akay, M. Non-calcified coronary atherosclerotic plaque characterization by dual energy computed tomography. *IEEE journal of biomedical and health informatics* **18**, 939–945 (2013).
20. Wei, J. *et al.* Computerized detection of noncalcified plaques in coronary ct angiography: Evaluation of topological soft gradient prescreening method and luminal analysis. *Medical physics* **41**, 081901 (2014).
21. Masuda, T. *et al.* Machine-learning integration of ct histogram analysis to evaluate the composition of atherosclerotic plaques: validation with ib-ivus. *Journal of cardiovascular computed tomography* **13**, 163–169 (2019).
22. Zhao, F. *et al.* An automatic multi-class coronary atherosclerosis plaque detection and classification framework. *Medical & biological engineering & computing* **57**, 245–257 (2019).
23. Kelm, B. M. *et al.* Detection, grading and classification of coronary stenoses in computed tomography angiography. In *International Conference on Medical Image Computing and Computer-Assisted Intervention*, 25–32 (Springer, 2011).
24. Zreik, M. *et al.* A recurrent cnn for automatic detection and classification of coronary artery plaque and stenosis in coronary ct angiography. *IEEE transactions on medical imaging* **38**, 1588–1598 (2018).
25. Lee, M. C. H., Petersen, K., Pawlowski, N., Glocker, B. & Schaap, M. Tetris: Template transformer networks for image segmentation with shape priors. *IEEE transactions on medical imaging* **38**, 2596–2606 (2019).

26. Kumamaru, K. K. *et al.* Diagnostic accuracy of 3d deep-learning-based fully automated estimation of patient-level minimum fractional flow reserve from coronary computed tomography angiography. *European Heart Journal-Cardiovascular Imaging* (2019).
27. Freiman, M., Manjeshwar, R. & Goshen, L. Unsupervised abnormality detection through mixed structure regularization (msr) in deep sparse autoencoders. *Medical physics* **46**, 2223–2231 (2019).
28. Lessmann, N. *et al.* Deep convolutional neural networks for automatic coronary calcium scoring in a screening study with low-dose chest CT. In *Medical Imaging 2016: Computer-Aided Diagnosis*, vol. 9785, 978511 (International Society for Optics and Photonics, 2016).
29. Lessmann, N. *et al.* Automatic calcium scoring in low-dose chest ct using deep neural networks with dilated convolutions. *IEEE transactions on medical imaging* **37**, 615–625 (2017).
30. Cano-Espinosa, C., González, G., Washko, G. R., Cazorla, M. & Estépar, R. S. J. Automated agatston score computation in non-ecg gated ct scans using deep learning. In *Medical Imaging 2018: Image Processing*, vol. 10574, 105742K (International Society for Optics and Photonics, 2018).
31. de Vos, B. D. *et al.* Direct automatic coronary calcium scoring in cardiac and chest ct. *IEEE transactions on medical imaging* **38**, 2127–2138 (2019).
32. van Velzen, S. G. *et al.* Direct prediction of cardiovascular mortality from low-dose chest ct using deep learning. In *Medical Imaging 2019: Image Processing*, vol. 10949, 109490X (International Society for Optics and Photonics, 2019).
33. Guo, H., Kruger, U., Wang, G., Kalra, M. K. & Yan, P. Knowledge-based analysis for mortality prediction from CT images. *IEEE Journal of Biomedical and Health Informatics* **24**, 457–464 (2020).
34. LeCun, Y., Bottou, L., Bengio, Y. & Haffner, P. Gradient-based learning applied to document recognition. *Proceedings of the IEEE* **86**, 2278–2324 (1998).
35. Krizhevsky, A., Sutskever, I. & Hinton, G. E. Imagenet classification with deep convolutional neural networks. In *Advances in neural information processing systems*, 1097–1105 (2012).
36. Shin, H.-C. *et al.* Deep convolutional neural networks for computer-aided detection: Cnn architectures, dataset characteristics and transfer learning. *IEEE transactions on medical imaging* **35**, 1285–1298 (2016).
37. Carreira, J. & Zisserman, A. Quo vadis, action recognition? a new model and the kinetics dataset. In *proceedings of the IEEE Conference on Computer Vision and Pattern Recognition*, 6299–6308 (2017).

38. Tran, D., Bourdev, L., Fergus, R., Torresani, L. & Paluri, M. Learning spatiotemporal features with 3d convolutional networks. In *Proceedings of the IEEE international conference on computer vision*, 4489–4497 (2015).
39. Lin, T.-Y., Goyal, P., Girshick, R., He, K. & Dollár, P. Focal loss for dense object detection. In *Proceedings of the IEEE international conference on computer vision*, 2980–2988 (2017).
40. He, K., Zhang, X., Ren, S. & Sun, J. Deep residual learning for image recognition. In *Proceedings of the IEEE conference on computer vision and pattern recognition*, 770–778 (2016).
41. Kingma, D. P. & Ba, J. Adam: A method for stochastic optimization. *arXiv preprint arXiv:1412.6980* (2014).
42. Hanley, J. A. & McNeil, B. J. The meaning and use of the area under a receiver operating characteristic (roc) curve. *Radiology* **143**, 29–36 (1982).
43. Zhou, X.-H., McClish, D. K. & Obuchowski, N. A. *Statistical methods in diagnostic medicine*, vol. 569 (John Wiley & Sons, 2009).
44. Chihara, L. & Hesterberg, T. *Mathematical statistics with resampling and R* (Wiley Online Library, 2011).

## Acknowledgments

This work was partly supported by National Heart, Lung, and Blood Institute (NHLBI) of the National Institutes of Health (NIH) under award R56HL145172. The authors thank the National Cancer Institute (NCI) for access to NCI's data collected by the National Lung Screening Trial. The statements contained herein are solely those of the authors and do not represent or imply concurrence or endorsement by NCI.

## Author contributions

G.W., M.K.K. and P.Y. initiated and supervised the project, and provided the concept and design of the experiments. H.C., H.S., G.W. and P.Y. developed the network architecture and analyzed the data. H.C. trained the network and reported the results with figures and tables. H.S. contributed machine learning expertise in network design and CT image analysis. F.H., R.S., R.D.K. and M.K.K. provided clinical expertise, acquired and annotated the MGH dataset, and screened NLST LDCT images. H.G. advised on data processing and performed additional experiments of a benchmark method. T.C. contributed on data curation. H.C. H.S., G.W., M.K.K. and P.Y. wrote the manuscript. All the authors reviewed and revised the manuscript.

## Methods

**The NLST dataset** The National Lung Screening Trial (NLST) enrolled 26,722 participants to undergo three annual screening exams with LDCT. We used 33,457 CT volumes from 10,400 subjects (for more details, see Fig. 5). They were randomly divided into training (7,272, 70%), validation (1,042, 10%) and test sets (2,086, 20%). The participants were enrolled in the trial from August 2002 through April 2004. Subject health history, reports of the annual LDCT screening scan and death information were collected through December 31, 2009. The NLST was approved by the institutional review board (IRB) at each of 33 participating medical institutions. The NLST data are publicly available through the Cancer Data Access System (CDAS) of the National Institutes of Health (NIH). LDCTs were collected from multiple institutions, with slice spacing varying from 0.5mm to 5mm. For a better longitudinal resolution, scans with slice spacing larger than 3mm were filtered out. Fig. 5 shows the inclusion and exclusion. Other properties of the NLST dataset are summarized in Table 1.

As the NLST is a study designed for lung cancer screening, CVD risk scores are not readily available. In order to train our model using the pipeline shown in Fig. 4, binary labels, abnormal and normal, were generated for the included subjects based on their health history, LDCT exam reports, and cause of death if available. Specifically, a subject was labeled as *normal*, if there had no cardiovascular abnormality known from either health history or LDCT reports, and the subject did not die of CVD during the trial and the follow-up period. A subject was labeled as *abnormal*, if any cardiovascular abnormality was reported during the screening trial in LDCT reports, or if the death certificate contains CVD related codes when the subject passed away during the trial or the follow-up period.

**The MGH dataset** The MGH dataset was collected at Massachusetts General Hospital (MGH at Boston, MA) in 2019. The retrospective study was approved by IRB with the waiver of informed consent. It was also performed in compliance with the Health Insurance Portability and Accountability Act (HIPAA). By reviewing the electronic medical records (EPIC, Epic Systems Corporation) at MGH, 119 adult patients were identified, who had clinically indicated LDCT for lung cancer screening as well as ECG-gated CT angiography and coronary calcium scoring within a 12-month period. Thirteen subjects were excluded because they had coronary stents, prosthetic heart valves, prior coronary artery bypass graft surgery, or metal artifacts in the region of cardiac silhouette. The final dataset contains 106 adult patients with details in Table 1. The data collected from each participant contains one chest LDCT image, one non-contrast ECG-gated cardiac CT (CCT) image, a CAC score (Agatston score)<sup>3</sup>, a Coronary Artery Disease Reporting and Data Systems (CAD-RADS<sup>TM</sup>) score<sup>4</sup> semi-automatically calculated from the CCT image, and a MESA 10-year risk score (MESA score)<sup>5</sup> calculated with the standard clinical protocol. LDCTs were reconstructed at 1-1.25 mm section thickness at 0.8-1 mm section interval using vendor-specific iterative reconstruction techniques (ASiRv, GE; iDose 4, Philips; ADMIRE, Siemens). It is noteworthy that the MGH dataset was not used for training or fine-tuning our proposed network, but only for evaluating/testing the performance of the deep learning model on LDCT to compare with

human experts defined standards from CCT.

**Model development** Challenges of chest LDCT based CVD risk estimation mainly come from three aspects. First, while a chest LDCT image volume has a large field view, the heart takes only a small subset. Features extracted by a deep learning model on the entire image may hide the CVD risk related information<sup>33</sup>. To tackle this problem, a cardiac region extractor was developed to locate and isolate the heart so that the risk estimation model can focus on this region of interest. Second, chest LDCT images are inherently 3D. In deep learning, 3D convolution neural networks (3D-CNNs) are needed for 3D feature extraction. However, popular 3D-CNN methods are either hard to train because of a huge amount of parameters<sup>37</sup> like C3D<sup>38</sup>, or need pretrained 2D-CNNs for parameter initialization like I3D<sup>37</sup>. At the same time, radiologists typically view CT images in 2D using the three orthogonal views: axial, sagittal, and coronal planes. Therefore, we designed a 3×2D network to efficiently extract features of 3D images in three orthogonal 2D views. The key details of the networks are presented as follows. Third, risk of CVD is hard to quantify. It could contain various diseases and symptoms. We combine information from various medical reports, including CT abnormalities reports, causes of death, and CVD histories, in NLST dataset and transfer the risk estimation task into a classification task. The whole pipeline of the proposed method is shown in Fig. 4.

- **Heart detector** RetinaNet<sup>39</sup> is used in our work to detect the heart region of interest. To train this network, we randomly selected 286 LDCT volumes from different subjects in the training set. We annotated the bounding boxes of the cardiac region including whole heart and aorta slice by slice in the axial view. In application, the trained detector is applied to each axial slice for independent localization. Then, the two extreme corner points  $A(x_{min}, y_{min}, z_{min})$  and  $B(x_{max}, y_{max}, z_{max})$  are identified by finding the maximal and minimal coordinates in all the detected bounding boxes, which defines the region enclosing the heart and excluding most of irrelevant anatomical structures.
- **CVD risk prediction model** As shown in Fig. 4, the proposed Tri2D-Net works in two stages, the feature extraction stage and the feature fusion stage. The feature extraction stage consists of three 2D CNN branches to extract features from the three orthogonal views independently. The parameters are not shared across these three networks. By setting a cross-entropy loss for each branch, the three 2D CNN branches can each separately receive direct feedback to learn the parameters. That is a significant advantage over training a massive 3D network, leading to a dramatically reduced optimization space. The 2D CNN branches are based on Resnet-18<sup>40</sup>. Specifically, in each branch, we split the original Resnet-18t into two parts, the first 13 layers (L13) and the last 5 layers (L-5). First, the L13 is employed on each slide separately, meaning each slide will have an extracted feature map. Then, a max pooling is employed on the slide dimension to fuse all these feature maps into one feature map. Finally, the feature map is feed to L-5 to form the representation of this view. In the feature fusion stage, the three feature representations extracted by the 2D CNN branches are concatenated and fed into a classifier for the final prediction.

- **Training and test details** The detected cardiac region is cut out from the original LDCT volume and resized to  $128 \times 128 \times 128$  with Gaussian smoothing. All the loss functions in the model are the cross-entropy loss. The model was trained with the Adam optimizer<sup>41</sup>. The learning rate was set to  $1 \times 10^{-4}$ . No learning rate decay strategy was applied. The model was trained 10,000 iterations with batch size of 32. Checkpoints of the model were saved every 100 iterations in the training stage. Then, the checkpoint achieved the highest performance on the NLST validation subset was selected as the final model. Data augmentations were used in all training, validation and test phases. In the training, an input  $128 \times 128 \times 128$  3D image was randomly cropped into  $112 \times 112 \times 112$ . In the validation and test phases, an input 3D image was augmented into 8  $112 \times 112 \times 112$  images with respect to 8 vertexes. The final classification probability is the average of 8 outputs. All models were trained, validated and tested on NVIDIA DGX-1 with 8 NVIDIA TESLA v100 GPUs.

**Statistical analysis** All confidence intervals of AUC values were computed based on the method proposed by Hanley et al.<sup>42</sup>. P values for significance testing on the AUC comparison were calculated based on the  $z$ -test described by Zhou et al.<sup>43</sup>. P values for sensitivity comparisons were calculated through a standard permutation test<sup>44</sup> with 10,000 random resamplings.

### **Data availability**

This study used the NLST dataset, which is publicly available at <https://biometry.nci.nih.gov/cdas/learn/nlst/images/>. The dataset from Massachusetts General Hospital was used under a research agreement for the current study, and is not publicly available.

### **Code availability**

The code used for training the models will be made publicly available at <https://github.com/dial-rpi/dl-cvd>.

## Supplementary material

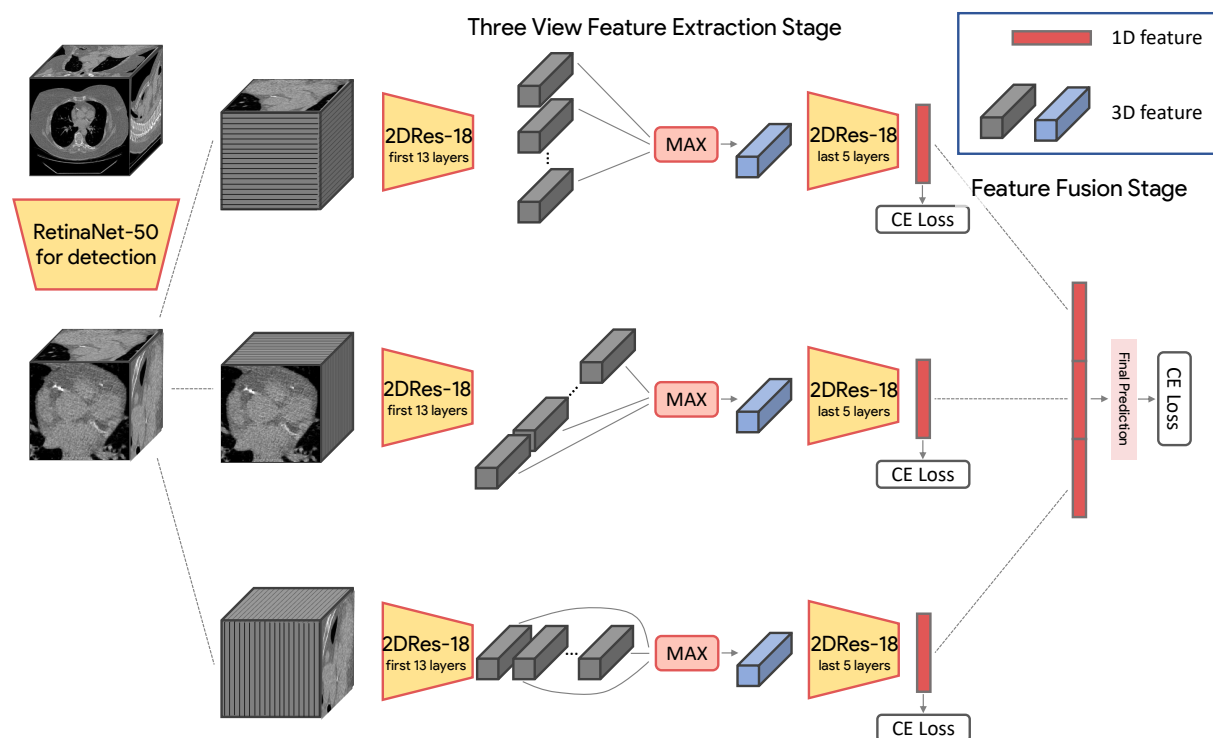


Figure 4: Framework of the proposed deep learning model - Tri2D-Net. The network contains two stages: the feature extraction stage and the feature fusion stage. The feature extraction stage consists of three 2D CNN branches to extract features from the three sequences of orthogonal views. The feature fusion stage aggregates the extracted features for classification.



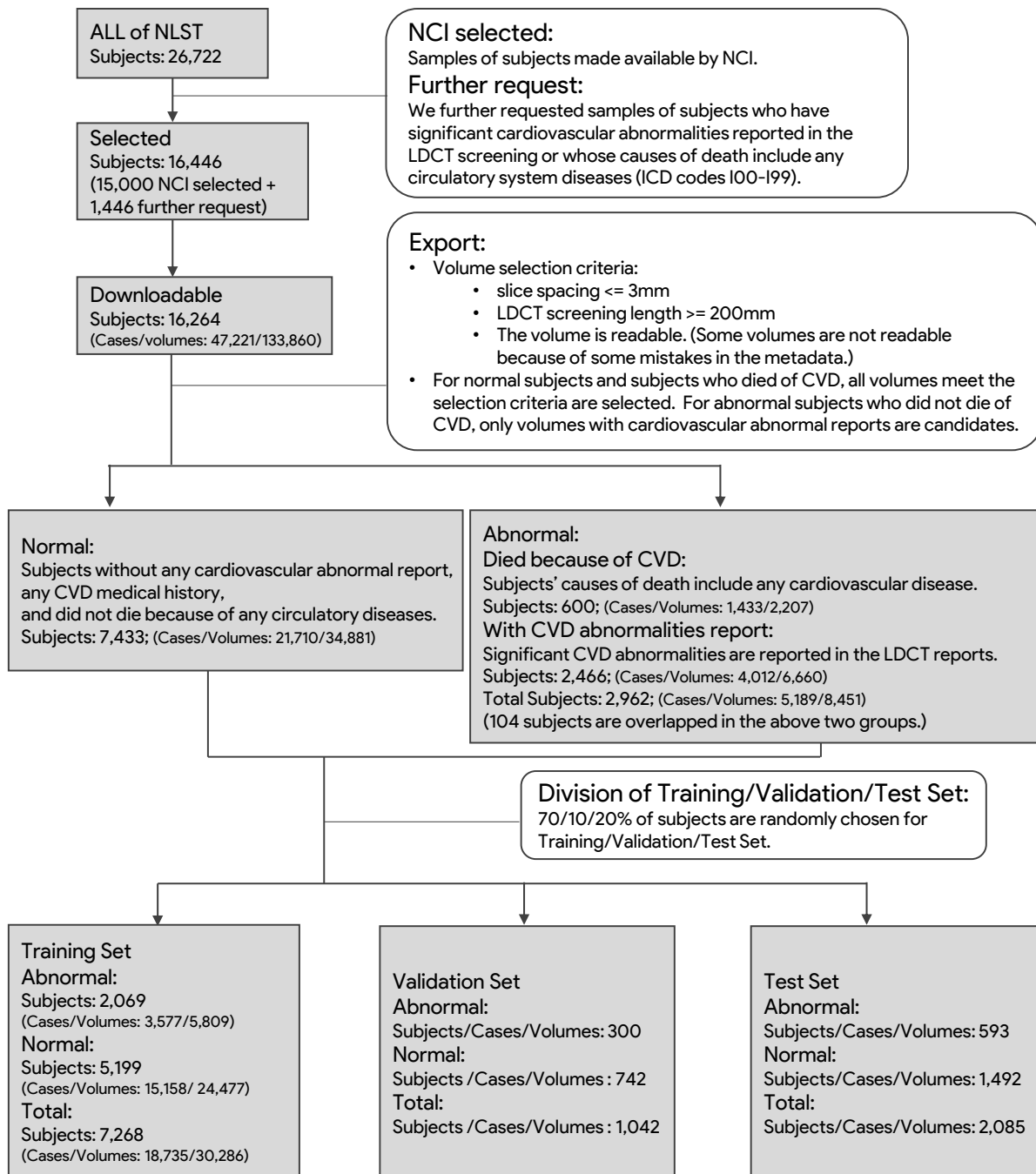
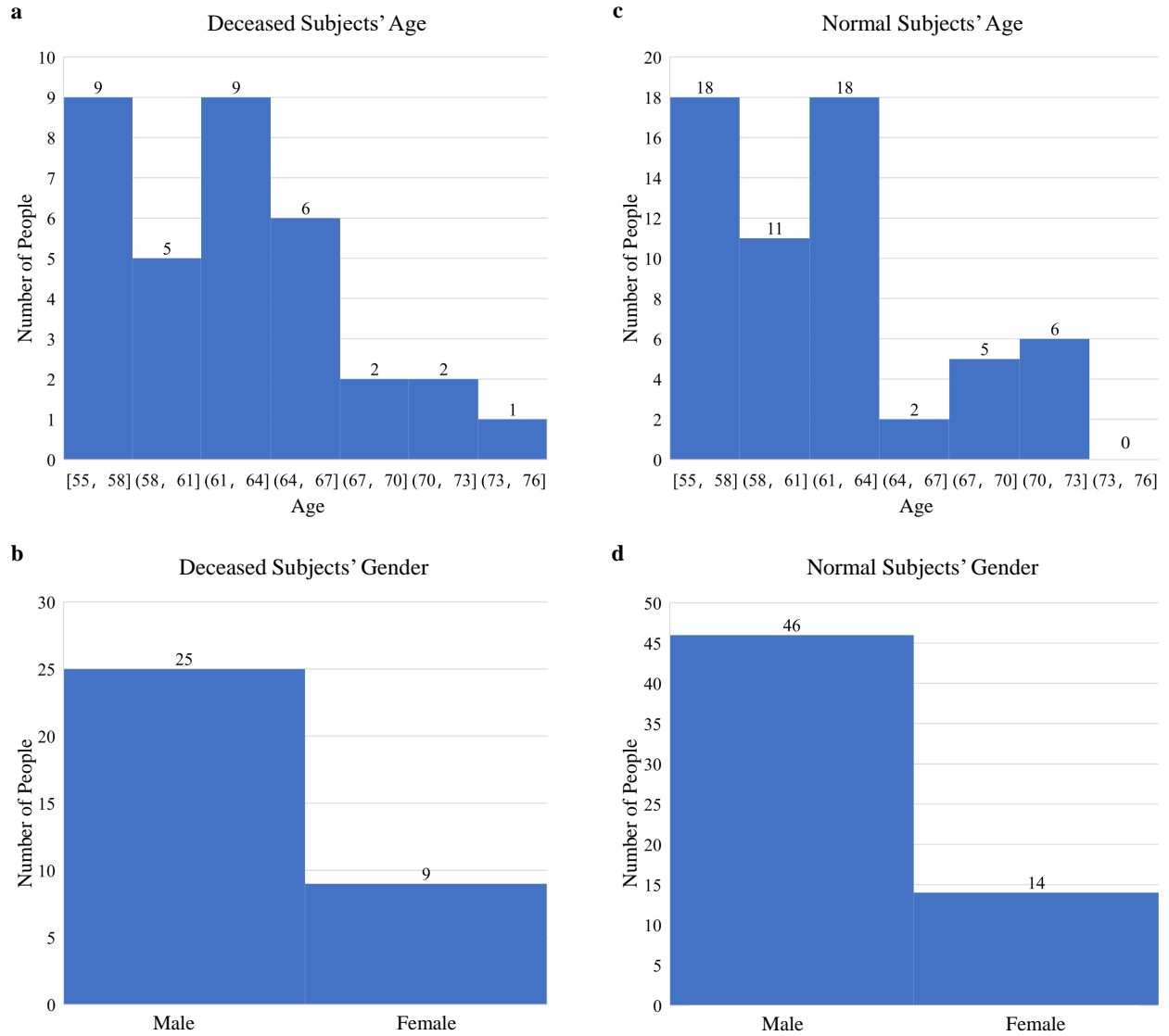


Figure 5: STARD flow diagram of the inclusion and exclusion of images in the NLST dataset used in our analysis.

Table 1: Characteristics of the two independent datasets used in our study. The numbers inside the parentheses are the number of exams performed on the subjects.

Dataset	NLST LDCT	MGH LDCT	MGH CCT
No. of subjects / exams	10,395 / 21,862	106	
Men	6,115 / 12,531	68	
Women	4,280 / 9,331	38	
Age (years)	61.4 $\pm$ 5 (54 $\sim$ 74)	64 $\pm$ 7 (55 $\sim$ 80)	
BMI Buckets			
Underweight $\leq 18.5$	150 / 304	0	
Normal (18.5 , 25]	3,331 / 7,210	17	
Overweight (25 , 30]	4,400 / 9,182	40	
Obese I (30 , 35]	1,854 / 3,857	36	
Obese II & III $> 35$	660 / 1,309	13	
CT Scan Setting			
Tube Voltage (kVp)	120 / 140	120	120
Tube Current (mA)	104.33 $\pm$ 41.48	91.05 $\pm$ 46.16	286.63 $\pm$ 167.38
Slice Thickness (mm)	1.98 $\pm$ 0.38	0.8 / 1.0	1.5
In-plane Resolution (mm)	0.656 $\pm$ 0.069	0.834 $\pm$ 0.091	0.341 $\pm$ 0.037



**Figure 6: Age and gender distributions of selected subjects without significant cardiac calcium from the NLST Dataset. a, Age distribution of the 34 deceased subjects. b, Gender distribution of the 34 deceased subjects. c, Age distribution of the 60 normal subjects. d, Gender distribution of the 60 normal subjects.**